ChemComm

COMMUNICATION

View Article Online
View Journal

Cite this: DOI: 10.1039/d4cc04926h

Received 23rd September 2024,
Accepted 11th November 2024

DOI: 10.1039/d4cc04926h

rsc.li/chemcomm

Acid-induced fluorescence enhancement of piperazinylphenyl-substituted nanographene†

Hao Zhao, [a] Rafael Muñoz-Mármol, [bc] Liliia Moshniaha, [d] Qiqi Yang, [e] Mischa Bonn, [e] Xiaomin Liu, [e] Ryota Kabe, [d] Giuseppe Maria Paternò *[cf] and Akimitsu Narita *[ae]

A dibenzo[*hi*,*st*]ovalene (DBOV) derivative bay-substituted with two piperazinylphenyl (PZP) groups (DBOV–PZP) was synthesized. Comprehensive investigations of its photophysical properties revealed acid-induced fluorescence enhancement through the protonation of PZP units, leading to the suppression of the photo-induced electron transfer. These results pave the way towards "turn-on" type nanographenes for biosensing and optical imaging.

Optical super-resolution imaging by single-molecule localization microscopy (SMLM)[1,2] has enabled the visualization of nanostructures with unprecedented resolutions in life and material science.[3,4] The key to realizing SMLM is the use of so-called blinking fluorophores, which enable precise localization of single molecules and the generation of high-quality images. Small-molecule dyes (*i.e.*, cyanine, rhodamine, and oxazine) are commonly used in SMLM,[5] but, their blinking performance is heavily environment-dependent, requiring external buffer.[5] Moreover, these dyes typically suffer from low photostability, restricting their applicability, *e.g.*, for live-cell imaging.[6] Organic fluorophores with self-blinking properties, without the need for the blinking buffer, have been demonstrated for the SMLM, but reported examples remain limited.[7]

Nanographenes, *i.e.*, large polycyclic aromatic hydrocarbons (PAHs), exhibit structure-dependent optical and electronic properties with considerable potential for applications in photonics and optoelectronics.[8] Nanographenes have also been considered for bioapplications, *e.g.* demonstrating high efficiency for photodynamic[9] and photothermal[10] cancer therapies and self-assembly to a functional platform for bioprobing.[11] Recently, we reported dibenzo[*hi*,*st*]ovalene (DBOV) as a highly stable and red-emissive nanographene that can serve as a self-blinking fluorophore toward super-resolution bioimaging by SMLM.[12] Live-cell SMLM imaging of lysosome dynamics was achieved, and a clickable DBOV derivative with azide group allowed single-molecule labeling and precise localization of nascent proteins in neurons, demonstrating great promise for further applications in life science.[13] However, the "always-on" fluorescence of DBOV prevented effective SMLM imaging by generating nonspecific background signals, which affect localization accuracy and specificity. It is crucial to develop analyte-sensitive nanographenes, especially with the "turn-on" type emission.

While nitrogen-doping can make nanographenes sensitive to acid and some metal ions, usually leading to quenched fluorescence,[14,15] boron-doped nanographenes can interact with Lewis bases, such as fluoride ions and pyridine, causing modulation of the fluorescence wavelengths.[16–18] However, such heteroatom-doping is often synthetically challenging and only applicable to specific analytes. To this end, edge functionalization can potentially provide easier access to nanographenes sensitive to various analytes, but reported examples are still rare and limited to the "turn-off" type,[19] to the best of our knowledge.

Piperazinylphenyl (PZP) groups have been demonstrated to serve as acid-responsive moieties for the development of "turn-on" type organic fluorophores.[20–22] PZP groups can quench the fluorescence of the parent fluorophore through the photoinduced electron transfer (PET), which becomes prohibited after the protonation to allow the fluorescence only under acidic conditions. In this work, we synthesized 1-methylpiperazinylphenyl-substituted DBOV (DBOV–PZP **3**) and studied its acid-sensitive optical properties (Fig. 1). Although the fluorescence of DBOV–PZP **3** was not completely suppressed, protonation of **3** led to the clear and reversible enhancement of the red emission. In-depth

[a] *Organic and Carbon Nanomaterials Unit, Okinawa Institute of Science and Technology Graduate University, 1919-1 Tancha, Onna-son, Kunigami-gun, Okinawa 904-0495, Japan*
[b] *Instituto Universitario de Materiales, University of Alicante, San Vicente del Raspeig 03690, Spain*
[c] *Physics Department, Politecnico di Milano, Piazza L. da Vinci 32, 20133 Milano, Italy. E-mail: giuseppemaria.paterno@polimi.it*
[d] *Organic Optoelectronics Unit, Okinawa Institute of Science and Technology Graduate University, 1919-1 Tancha, Onna-son, Kunigami-gun, Okinawa 904-0495, Japan*
[e] *Max Planck Institute for Polymer Research Ackermannweg 10, 55128 Mainz, Germany. E-mail: narita@mpip-mainz.mpg.de*
[f] *Center for Nanoscience and Technology, Istituto Italiano di Tecnologia, Milano 20134, Italy*

† Electronic supplementary information (ESI) available. See DOI: https://doi.org/10.1039/d4cc04926h

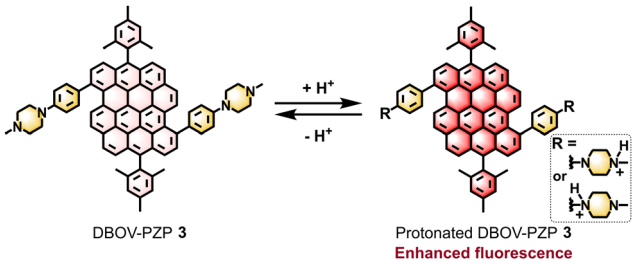

Fig. 1 Acid-promoted fluorescence enhancement of DBOV–PZP **3** through the protonation of PZP units, suppressing the PET.

investigations of the photophysical properties of **3**, involving ultrafast transient absorption (TA) spectroscopy, pointed to the population of an emissive intramolecular charge-transfer (ICT) state, which was suppressed by the protonation. These results pave the way towards "turn-on" type nanographenes for biosensing and optical imaging.

For the synthesis of **3**, PZP-boronic ester **2** was prepared by Miyaura–Ishiyama borylation of 1-(4-bromophenyl)-4-methylpiperazine **4** in 62% yield (Scheme S1 and Fig. S1, S2, ESI†). Then, Suzuki–Miyaura coupling of 3,11-dibromo-substituted DBOV **1** and **2** afforded **3** in 26% yield (Fig. 2a). ^{1}H NMR spectrum of **3** revealed sharp and well-resolved peaks (Fig. 2b), which were consistent with the spectra of PZP-boronic ester **2** and previously reported DBOV derivatives[23–25] (Fig. S3–S8, ESI†). High-resolution matrix-assisted laser desorption/ionization time-of-flight mass spectrometry (HR MALDI-TOF MS) analysis of **3** exhibited an intense peak with *m*/*z* of 1056.5109, in agreement with the calculated exact mass of 1056.5131 with an error of −2.1 ppm (Fig. 2c and Fig. S9, ESI†). Moreover, the experimental isotopic distribution (black) was fully consistent with the simulated pattern (red). These results validated the successful synthesis of **3**.

The optical properties of DBOV–PZP **3** were investigated by UV-vis absorption and fluorescence spectroscopy in different solvents, also measuring fluorescence lifetimes and

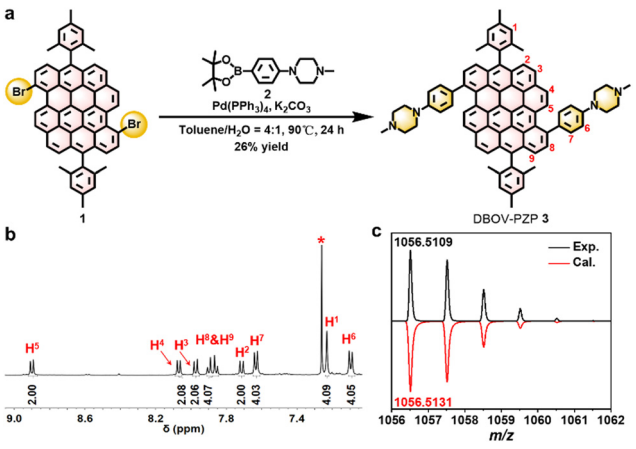

Fig. 2 (a) Synthesis of DBOV-PZP **3**. (b) Aromatic region of the ^{1}H NMR spectrum of **3** in $CDCl_3$ (500 MHz, 293 K). The solvent peak is marked with an asterisk. (c) HR MALDI-TOF MS spectrum of **3**, showing the isotopic distribution in comparison with a pattern stimulated for $C_{78}H_{64}N_4$.

photoluminescence quantum yields (PLQYs). The UV-vis absorption spectrum of **3** in methanol (MeOH) revealed an absorption maximum ($\lambda_{abs.}$) at 626 nm, which slightly red-shifted up to 642 nm in other organic solvents, including dichloromethane (DCM), toluene (Tol), chlorobenzene (CB), pyridine (Py), and dimethylformamide (DMF) (Fig. S9, S10 and Table S1, ESI†). Notably, the red-shift of $\lambda_{abs.}$ was roughly in accordance with increasing solvent polarity, indicating its solvent polarity-dependent photophysical properties.[26] In line with the previously reported DBOV derivatives.[23,25] DBOV–PZP **3** exhibited strong red emission, showing an emission maximum (λ_{em}) at 671 nm with a relatively large Stokes shift[24] of 45 nm (1071 cm^{-1}) in MeOH. Interestingly, **3** displayed shoulder peaks at ∼730–743 nm in low-polarity solvents (*i.e.*, Tol, DCM, and CB), which became featureless in high-polarity solvents, especially in Py and DMF (Fig. S9, S10 and Table S1, ESI†). Moreover, considerable red-shift of λ_{em}, increased Stokes shift, decreased fluorescence lifetimes, and smaller PLQYs were observed for **3** in solvents with higher polarity (Fig. S10–S14 and Table S1, ESI†), indicating the ICT character of its emission.[27] Moreover, excitation emission matrix spectra (EEMs) of **3** revealed the excitation wavelength-independent nature of the emission peaks at ∼650–750 nm (Fig. S15, ESI†).

The acid responsiveness of DBOV–PZP **3** was investigated by monitoring the changes in UV-vis absorption and fluorescence spectra in MeOH upon titration with hydrochloric acid (HCl). In contrast to the negligible variation in UV-vis absorption spectra (Fig. S16, ESI†), the fluorescence intensity at λ_{em} started to increase upon the addition of 0.6 equivalent (eq.) of HCl, reaching a plateau after adding 2.0 eq. of HCl, eventually achieving a ∼1.8-fold increment (Fig. 3a and c). Simultaneously, a blue-shift of the λ_{em} from 671 to 658 nm and a slight decrement of the fluorescence intensity at the tail of the spectra were also observed, resulting in an equivalent point at ∼740 nm. An excess of HCl (6.0 eq.) did not change the spectra, indicating the complete protonation of DBOV–PZP **3** with 2.0 eq. of HCl. Furthermore, the enhanced fluorescence could be attenuated along with the red-shift of λ_{em} to the initial state by progressively adding triethylamine (TEA) up to 6.0 eq., which neutralizes the protonated DBOV–PZP **3** (Fig. 3b and c). Moreover, the changes in fluorescence spectra were contiguously monitored upon subsequently adding 9.0 eq. of TEA, revealing a slightly quenched fluorescence and further red-shift of λ_{em} for DBOV–PZP **3** under basic conditions. Notably, the PLQY and lifetime of **3** were measured to be ∼0.40 and ∼5.0 ns, respectively, which increased to ∼0.60 and ∼6.3 ns after adding 6 eq. of HCl, and then decreased to ∼0.36 and ∼4.7 ns, respectively, upon the addition of 12 eq. of TEA (Fig. 3d, e and Fig. S17, S18, ESI†). The structure and coordinates of the peaks in the EEMs of DBOV–PZP **3** did not change, but a higher fluorescence intensity was observed in the acidic condition (1970 a.u.) in comparison to that in neutral (1195 a.u.) and basic (965 a.u.) solutions (Fig. S19, ESI†), in agreement with the observed fluorescence behavior (Fig. 3a–c). These results were attributed to the prohibited and favorable PET in acidic and basic conditions, respectively, resulting in enhanced and suppressed

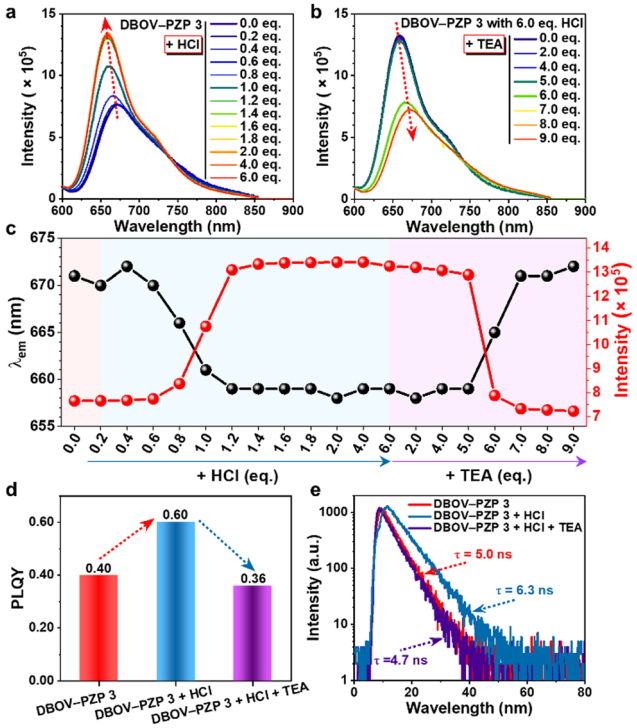

Fig. 3 (a) Changes in the fluorescence spectra of DBOV–PZP **3** (5×10^{-6} M in MeOH) upon titration with (a) HCl and (b) TEA, as well as (c) the variations of the corresponding fluorescence maximum and intensity during the titration. Comparison of (d) PLQY and (e) emission decay profiles of DBOV–PZP **3** (2.5×10^{-6} M in MeOH), after the addition of 6 eq. of HCl, followed by neutralizing the mixture with 12 eq. of TEA.

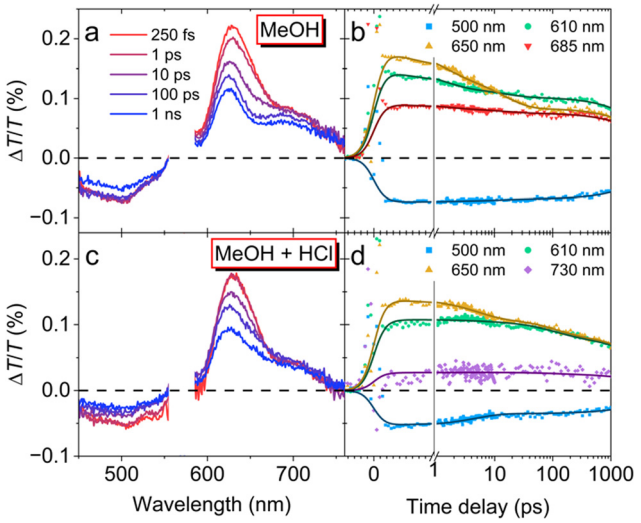

Fig. 4 Differential transmission ($\Delta T/T$) spectra at various time delays between pump and probe for DBOV-PZP **3** in MeOH (1.9×10^{-4} M) (a) before and (c) after adding excess HCl. Transient dynamics at relevant wavelengths matching ESA (500 nm, blue squares), GSB (610 nm, green circles) and SE (650 nm, orange up-triangles; 685 nm, red down-triangles; and 730 nm, purple diamonds) for **3** in MeOH (b) before and (d) after adding 6 eq. of HCl. Full lines are exponential fits to the data. The sample was excited at λ_{pump} = 570 nm with a 70-fs pulse, power P_{pump} = 200 mW cm^{-2} at 1 kHz repetition rate.

fluorescence. On the other hand, these data also revealed the acid-induced fluorescence enhancement and reversible protonation/deprotonation process of DBOV–PZP **3**, indicating its proton-sensing ability.

Ultrafast transient absorption (TA) spectroscopy was next performed to gain further insight into the excited state photophysical properties of DBOV–PZP **3** (Fig. 4). The TA spectra of **3** in MeOH (Fig. 4a) present positive peaks at 625 and 570 nm, matching the ground state absorption that corresponds with an increase of the transmitted probe generated by the depletion of the ground state population after excitation, also known as ground state bleaching (GSB). Then, the TA spectrum captured right after excitation (250 fs) presents the typical characteristics associated with singlet excited state: (i) a negative band at 500 nm generated by the promotion of excited state population to higher lying states-*i.e.*, excited state absorption (ESA)-and (ii) positive peak close to 730 nm due to stimulated emission (SE), which also contribute to the 625-nm-peak. Notice that such initial SE resembles the PL spectrum of DBOV–PZP **3** in non-polar solvents. Then, as the delay time increases, the SE contribution from the singlet excited state quickly decays, evolving into a broad featureless band centered at 685 nm that matches the PL spectrum of **3** in polar solvents. The spectral evolution was corroborated by normalizing the spectra to their maxima (Fig. S20, ESI†). The new state is presumably assignable to the emissive ICT state. Additionally, such evolution can be clearly followed in Fig. 4b, where 610 and 650 nm were selected to disentangle the contributions from the GSB and SE, respectively. The GSB (610 nm) is proportional to the population that remains excited at each time delay, while the major contribution to the SE at 650 nm comes from the singlet excited state. Their completely different dynamics reveal two extra components in the decay of the initial singlet excited population (1.3 and 15 ps) that might correspond with the molecular rearrangement and PET to the emissive ICT state, from which the population finally decays with a 5.2 ns time constant.

The same analysis was conducted with DBOV–PZP **3** in MeOH (1.9×10^{-4} M) after adding excess HCl. This time, the TA spectra shown in Fig. 4c display the characteristic features associated with the singlet excited state population-ESA at 500 nm and SE at 730 and 626 nm-independently of the time delay. A slightly faster decay of the SE can be appreciated only after normalizing the TA spectra to their respective maxima (Fig. S20, ESI†). Clearly, HCl inhibits the formation of the ICT state. The dynamics in Fig. 4d further prove this point. Finally, the dynamics at 650 nm-associated with singlet excited state population-decays with a 5.6 ns time constant with only small contributions from molecular rearrangement (4.8 ns) and other possible non-radiative channels (110 ps). The larger decay found after adding the HCl, *i.e.* 5.6 ns *versus* 5.2 ns, is also compatible with the differences found in their PL lifetimes.

Finally, DBOV–PZP **3** was found to show photoblinking, which enables applications for super-resolution SMLM imaging. Blinking properties (photon number, blinking time, and on–off duty cycle) were investigated in air and after adding HCl (Fig. S21 and S22, ESI†), demonstrating excellent blinking

properties comparable to the gold standard dye Alexa 647 under both conditions.[5] A small increase in the number of photons could be observed after adding HCl, implying acid-induced modulation of the blinking properties. As a proof-of-concept, SMLM imaging of nanoscale crevices in a glass substrate was achieved with DBOV–PZP **3** (Fig. S23, ESI†), although further improvements in the sensitivity will be necessary for SMLM-based pH sensing.

In summary, we have achieved the synthesis of DBOV–PZP **3** and demonstrated its acid-induced fluorescence enhancement through the protonation of PZP units. Fluorescence spectroscopy revealed the reversible enhancement of the red emission, indicating its proton-sensing ability. Ultrafast TA spectroscopy elucidated the population of an emissive ICT state upon excitation of DBOV–PZP **3**, which was prohibited after the protonation, accounting for the promoted fluorescence. Moreover, **3** exhibited excellent self-blinking properties enabling the SMLM imaging. This work thus paves the way towards the development of ''turn-on'' type nanographenes for super-resolution biosensing and bioimaging applications.

This work was supported by the Okinawa Institute of Science and Technology Graduate University (OIST), JSPS KAKENHI Grant No. JP21J01147, JP23KF0075, and the Max Planck Society. H. Zhao acknowledges the JSPS Postdoctoral Fellowship for Research in Japan. G. M. Paternò receives funding from the European Union (ERC, EOS, 101115925) and from the Next-GenerationEU Programme with the IPHOQS Infrastructure [IR0000016, ID D2B8D520, CUP B53C22001750006] ''Integrated Infrastructure Initiative in Photonic and Quantum Sciences''. R. Muñoz-Mármol acknowledges the financial support from the University of Alicante, Spanish Ministry of Universities and European Union-Next Generation EU for its Margarita Salas Fellowship (MARSALAS22-18). We also appreciate the help and support provided by the Instrumental Analysis Section of Research Support Division at OIST. Open Access funding provided by the Max Planck Society.

Data availability

Data for this article are available at Zenodo at **https://doi.org/10.5281/zenodo.13827689** or in the ESI.†

Conflicts of interest

X. Liu, A. Narita, and M. Bonn are listed as inventors on a patent (PCT/EP2019/076496, WO2020070085) related to this work. All other authors have nothing to disclose.

Notes and references

1 E. Betzig, G. H. Patterson, R. Sougrat, O. W. Lindwasser, S. Olenych, J. S. Bonifacino, M. W. Davidson, J. Lippincott-Schwartz and H. F. Hess, *Science*, 2006, **313**, 1642–1645.
2 M. J. Rust, M. Bates and X. Zhuang, *Nat. Methods*, 2006, **3**, 793–796.
3 S. Pujals, N. Feiner-Gracia, P. Delcanale, I. Voets and L. Albertazzi, *Nat. Rev. Chem.*, 2019, **3**, 68–84.
4 S. J. Sahl, S. W. Hell and S. Jakobs, *Nat. Rev. Mol. Cell Biol.*, 2017, **18**, 685–701.
5 G. T. Dempsey, J. C. Vaughan, K. H. Chen, M. Bates and X. Zhuang, *Nat. Methods*, 2011, **8**, 1027–1036.
6 S.-N. Uno, M. Kamiya, T. Yoshihara, K. Sugawara, K. Okabe, M. C. Tarhan, H. Fujita, T. Funatsu, Y. Okada and S. Tobita, *Nat. Chem.*, 2014, **6**, 681–689.
7 X. Gu, E. Zhao, T. Zhao, M. Kang, C. Gui, J. W. Y. Lam, S. Du, M. M. T. Loy and B. Z. Tang, *Adv. Mater.*, 2016, **28**, 5064–5071.
8 G. M. Paternò, Goudappagouda, Q. Chen, G. Lanzani, F. Scotognella and A. Narita, *Adv. Opt. Mater.*, 2021, **9**, 2100508.
9 H. A. Lin, Y. Sato, Y. Segawa, T. Nishihara, N. Sugimoto, L. T. Scott, T. Higashiyama and K. Itami, *Angew. Chem., Int. Ed.*, 2018, **57**, 2874–2878.
10 X.-H. Ma, X. Gao, J.-Y. Chen, M. Cao, Q. Dai, Z.-K. Jia, Y.-B. Zhou, X.-J. Zhao, C. Chu, G. Liu and Y.-Z. Tan, *J. Am. Chem. Soc.*, 2024, **146**, 2411–2418.
11 M. Yin, J. Shen, W. Pisula, M. Liang, L. Zhi and K. Müllen, *J. Am. Chem. Soc.*, 2009, **131**, 14618–14619.
12 X. Liu, S. Y. Chen, Q. Chen, X. Yao, M. Gelléri, S. Ritz, S. Kumar, C. Cremer, K. Landfester and K. Müllen, *Angew. Chem., Int. Ed.*, 2020, **59**, 496–502.
13 X. Zhu, Q. Chen, H. Zhao, Goudappagouda, Q. Yang, M. R. Gelléri, S. Ritz, D. Ng, K. Koynov and S. H. Parekh, *J. Am. Chem. Soc.*, 2024, **146**, 5195–5203.
14 S. M. Draper, D. J. Gregg and R. Madathil, *J. Am. Chem. Soc.*, 2002, **124**, 3486–3487.
15 E. Jin, Q. Yang, C.-W. Ju, Q. Chen, K. Landfester, M. Bonn, K. Müllen, X. Liu and A. Narita, *J. Am. Chem. Soc.*, 2021, **143**, 10403–10412.
16 K. Matsuo, S. Saito and S. Yamaguchi, *J. Am. Chem. Soc.*, 2014, **136**, 12580–12583.
17 S. Osumi, S. Saito, C. Dou, K. Matsuo, K. Kume, H. Yoshikawa, K. Awaga and S. Yamaguchi, *Chem. Sci.*, 2016, **7**, 219–227.
18 W. Sun, J. Guo, Z. Fan, L. Yuan, K. Ye, C. Dou and Y. Wang, *Angew. Chem., Int. Ed.*, 2022, **61**, e202209271.
19 V. Vij, V. Bhalla and M. Kumar, *ACS Appl. Mater. Interfaces*, 2013, **5**, 5373–5380.
20 D. Asanuma, Y. Takaoka, S. Namiki, K. Takikawa, M. Kamiya, T. Nagano, Y. Urano and K. Hirose, *Angew. Chem., Int. Ed.*, 2014, **53**, 6085–6089.
21 J. Zhang, M. Yang, C. Li, N. Dorh, F. Xie, F.-T. Luo, A. Tiwari and H. Liu, *J. Mater. Chem. B*, 2015, **3**, 2173–2184.
22 X. Zhang, Y. Yan, Q. Peng, J. Wang, Y. Hang and J. Hua, *Mater. Chem. Front.*, 2017, **1**, 2292–2298.
23 Q. Chen, S. Thoms, S. Stöttinger, D. Schollmeyer, K. Müllen, A. Narita and T. Basché, *J. Am. Chem. Soc.*, 2019, **141**, 16439–16449.
24 G. M. Paterno, Q. Chen, R. Muñoz-Mármol, M. Guizzardi, V. Bonal, R. Kabe, A. J. Barker, P. G. Boj, S. Chatterjee and Y. Ie, *Mater. Horiz.*, 2022, **9**, 393–402.
25 Q. Chen, D. Wang, M. Baumgarten, D. Schollmeyer, K. Müllen and A. Narita, *Chem. – Asian J.*, 2019, **14**, 1703–1707.
26 X. Xu, A. L. V. Haar, R. Yoshioka, Q. Zhang, S. Vasylevskyi, A. J. Musser and A. Narita, *Chem. Commun.*, 2023, **59**, 720–723.
27 A. M. Alvertis, S. Lukman, T. J. H. Hele, E. G. Fuemmeler, J. Feng, J. Wu, N. C. Greenham, A. W. Chin and A. J. Musser, *J. Am. Chem. Soc.*, 2019, **141**, 17558–17570.

